Inorganic Chemistry

ARTICLE

pubs.acs.org/IC

# Spacer-Dependent Structural and Physicochemical Diversity in Copper(II) Complexes with Salicyloyl Hydrazones: A Monomer and Soluble Polymers

Dariusz Matoga,* Janusz Szklarzewicz, Ryszard Gryboś, Katarzyna Kurpiewska, and Wojciech Nitek

Faculty of Chemistry, Jagiellonian University, Ingardena 3, 30-060 Kraków, Poland

Supporting Information

**ABSTRACT:** Complexation of copper(II) with a series of heterodonor chelating Schiff bases (LL) of salicylic acid hydrazide and aliphatic or cycloaliphatic ketones affords soluble one-dimensional (1D) metallopolymers containing Schiff bases as bridging ligands. Single-crystal X-ray diffraction results reveal nanometer-sized metallopolymeric wires $[Cu(\mu\text{-}LL)_2]_n$ with off-axis linkers and a zigzag geometry. Octahedrally coordinated copper centers, exhibiting a Jahn−Teller distortion, are doubly bridged by two Schiff-base molecules in the $\mu_2-\eta^1,\eta^2$ coordination mode. The use of dibutylketone with long alkyl chains as a component for Schiff base formation leads to a distorted square planar monomeric copper(II) complex $[Cu(LL)_2]$, as evidenced by its X-ray crystal structure. The compounds are characterized by elemental analyses and IR and UV−vis spectroscopy, as well as magnetic susceptibility and cyclic voltammetry measurements. Electrochemical studies on the complexes reveal an existence of polymeric and monomeric forms in solution and the dependence of Cu(II)/Cu(I) reduction potentials on alkyl groups of salicyloyl hydrazone ligands. Polymeric complexes form conducting films on Pt electrodes upon multicycle potential sweeps.

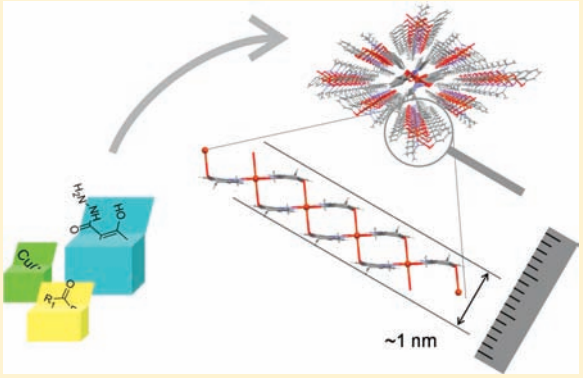


## INTRODUCTION

The synthesis of coordination polymers is an important field of chemistry with tremendous potential in the development of materials with desirable properties. The applications where metallopolymers may be used include, for instance, electronic, magnetic, and optoelectronic devices; advanced nanocomposites; or biological sensors.[1] These one-, two-, or three- dimensional systems may also be porous, which often translates to their further applications in gas storage and catalysis.[1] In this wide class of materials, the conjugated polymers incorporating metal complexes give rise to considerable interest among researchers, since they have potential to be electrically conducting and offer attractive magnetic, photochemical, optical, and electrical properties as well.[2,3] In addition, the solubility of metallopolymers is a valuable feature, because it enables their fuller characterization and it opens the possibility of their deposition as films on various surfaces. However, the preparation of soluble metallopolymers still remains a challenge.[1−3]

We recently became interested in coordination polymers based on copper(II) Schiff-base complexes that may exhibit porous and/or conducting properties. As a line of this study, we were investigating a series of salicyloyl hydrazones that, at first glance, seemed to act as normal bidentate ligands. However, our research, reported in this paper, has shown that these ligands may become bridging ones and are able to form interesting unusual single-chain copper-organic backbones.

In the literature, there are a few examples of polymeric Schiff-base copper(II) complexes investigated with relevance to potential applications in material science and functional devices. These supramolecular structures usually contain chelating Schiff-base ligands and the bridging between metal centers occurs either directly via this organic ligand[3−5] or via another, usually inorganic linker;[6,7] otherwise, mixed organic and inorganic bridges are observed.[8] Recently, a series of polymeric copper complexes was also reported with reduced Schiff base ligands and an example of the utilization of a two-dimensional (2D) copper(II) coordination polymer with one such ligand in the generation of CuS nanomaterial with hollow structures was presented.[9,10] In the group of Schiff-base copper(II) polymers, metal complexes with hydrazones are rare.[5,6] Despite their attractiveness as advanced materials, hydrazone ligands and their copper(II) complexes are also interesting as potential chemotherapeutic agents, since analogous systems were found to exhibit antitumor and antibacterial activities.[11,12]

In this work, we report on the synthesis and X-ray crystal structures, as well as spectroscopic and electrochemical properties of the series of soluble copper(II) polymers with salicyloyl hydrazone linkers. For comparison, a mononuclear complex is prepared and characterized with the use of dibutylketone as a

**Received:** December 8, 2010
**Published:** March 23, 2011

**Table 1. Crystal Data and Structure Refinement Parameters for 1, 2, and 4**

| | 1 | 2 | 4 |
|---|---|---|---|
| empirical formula | $C_{20}H_{22}N_4O_4Cu$ | $C_{22}H_{26}N_4O_4Cu$ | $C_{32}H_{46}N_4O_4Cu$ |
| formula weight | 445.79 | 474.01 | 613.91 |
| crystal size | 0.30 mm × 0.15 mm × 0.10 mm | 0.20 mm × 0.15 mm × 0.15 mm | 0.33 mm × 0.30 mm × 0.08 mm |
| crystal system | monoclinic | monoclinic | triclinic |
| space group | $P2_1/c$ | $P2_1/c$ | $P\bar{1}$ |
| $a$ | 6.22000(10) Å | 6.1507(2) Å | 8.1220(4) Å |
| $b$ | 16.2648(3) Å | 11.0663(4) Å | 9.3940(4) Å |
| $c$ | 10.5760(3) Å | 15.5218(5) Å | 11.9660(5) Å |
| α | 90.00° | 90.00° | 95.922(3)° |
| $\beta$ | 116.857(2)° | 96.195(3)° | 102.409(3)° |
| $\gamma$ | 90.00° | 90.00° | 114.530(2)° |
| $V$ | 954.53(4) Å$^3$ | 1050.33(6) Å$^3$ | 791.93(6) Å$^3$ |
| $Z$ | 2 | 2 | 1 |
| $T$ | 293(2) K | 110(2) K | 293(2) K |
| $D_c$ | 1.551 Mg/m$^3$ | 1.499 Mg/m$^3$ | 1.287 Mg/m$^3$ |
| $\mu$ | 1.180 mm$^{-1}$ | 1.077 mm$^{-1}$ | 0.731 mm$^{-1}$ |
| reflections measured | 5481 | 4461 | 6646 |
| reflections unique | 1946 | 2317 | 3610 |
| reflections observed [$I > 2\sigma(I)$] | 1664 | 1780 | 3243 |
| $R$ indices [$I > 2\sigma(I)$] | | | |
| $R$ | 0.0248 | 0.0374 | 0.055 |
| $wR_2$ | 0.0701 | 0.1066 | 0.1557 |
| $S$ | 1.088 | 1.059 | 1.051 |

hydrazone component. Its long alkyl groups make it become just a chelating ligand and not a bridging Schiff base ligand. All obtained polymeric nanostructures and the monomer are a unique example of spacer-dependent structural diversity in copper complexes. Since copper occurs commonly at redox active sites of metalloenzymes, where it shuttles between cuprous and cupric ions during biochemical processes, it is also of interest in this work to ascertain whether the salicyloyl hydrazone polymers can exist in both +1 and +2 oxidation states of copper and, if so, how readily the interconversion of the oxidation states can occur. The electrochemical behaviors of the polymeric complexes are also under scrutiny, with regard to electronic charge transfer within the metal−organic polymer backbones, as well as their ability to form conducting films.

## EXPERIMENTAL SECTION

Salicylic acid hydrazide and copper(II) acetate monohydrate were synthesized according to published methods.[13,14] All other chemicals and solvents were of analytical grade (Aldrich, Lach-ner, Reactivul-Bucuresti, Koch-Light Laboratories, Polmos) and were used as supplied. Carbon, hydrogen, and nitrogen contents were determined using an Elementar Vario MICRO Cube elemental analyzer. Solid samples for IR spectroscopy were compressed as KBr pellets, and the IR spectra were recorded on a Bruker EQUINOX 55 FT-IR spectrophotometer. Electronic absorption spectra were measured with a Shimadzu UV-3600 UV−vis-NIR spectrophotometer. Diffuse reflectance spectra were measured in $BaSO_4$ pellets, with $BaSO_4$ as a reference, using a Shimadzu Model 2101PC system equipped with an ISR-260 attachment. Magnetic susceptibility measurements were carried out at room temperature on a Sherwood Scientific Magway MSB MK1 balance. Cyclic voltammetry measurements were carried out in dimethylsulfoxide (DMSO) with $[Bu_4N]PF_6$ (0.10 M) as the supporting electrolyte, using Pt working and counter and Ag/AgCl reference electrodes on an AUTOLAB/PGSTAT 128N Potentiostat/Galvanostat. Cyclic voltammograms were obtained under argon at room temperature. $E_{1/2}$ values were calculated from the average anodic and cathodic peak potentials:

$$E_{1/2} = 0.5(E_a + E_c)$$

The redox potentials were calibrated versus ferrocene, which was used as an internal potential standard for measurements, to avoid the influence of liquid junction potential; the final values are reported versus a standard hydrogen electrode.

**Synthesis of [Cu($\mu$-acesah)$_2$]$_n$ (1).** Salicylic acid hydrazide (304 mg, 2.00 mmol) and acetone (140 $\mu$L, 2.00 mmol) were dissolved in EtOH (40 mL) and heated under reflux for ∼15 min. $[Cu(O_2CCH_3)_2]\cdot H_2O$ (200 mg, 1.00 mmol) was added and the heating under reflux of the resultant green suspension was continued for ∼5 min. Green precipitate of **1** (yield: 0.25 g, 55%) was filtered off, washed twice with small amount of cold EtOH, and dried in air at room temperature. Anal. Calcd for $C_{20}H_{22}N_4O_4Cu$: C, 53.87; H, 4.97; N, 12.56. Found: C, 53.58; H, 4.94; N, 12.32%. IR (KBr, cm$^{-1}$): $\nu_{CN(imine)}$, 1596(vs), 1623(m); $\nu_{CO(enolate)}$, 1253(s); $\nu_{CO(phenolic)}$, 1299(m). UV−vis (solid state) $\lambda$, nm: 600, 370(sh), 310, 270, 220. UV−vis [DMSO solution: $\lambda$, nm ($\varepsilon$, dm$^3$ mol$^{-1}$ cm$^{-1}$)]: 628 (120), 310 (7300). Green crystals of **1** suitable for single-crystal X-ray diffraction (XRD) were obtained after recrystallization from MeCN.

**Synthesis of [Cu($\mu$-emsah)$_2$]$_n\cdot 0.5n$H$_2$O (2·0.5$n$H$_2$O).** The synthetic procedure was analogous to that of **1**, except that ethylmethylketone (179 $\mu$L, 2.00 mmol) was used instead of acetone. (Yield: 0.28 g; 59%) Anal. Calcd for $C_{22}H_{27}N_4O_{4.5}Cu$: C, 54.70; H, 5.63; N, 11.60. Found: C, 54.32; H, 5.20; N, 11.96%. IR (KBr, cm$^{-1}$): $\nu_{CN(imine)}$, 1602(vs); $\nu_{CO(enolate)}$, 1257(vs); $\nu_{CO(phenolic)}$, 1329(m). UV−vis (solid state) $\lambda$, nm: 600, 370(sh), 310, 270, 220. UV−vis [DMSO solution: $\lambda$, nm ($\varepsilon$, dm$^3$ mol$^{-1}$ cm$^{-1}$)]: 636 (99), 310 (2300). Green crystals of **2** suitable for single-crystal XRD were obtained after recrystallization from MeCN.


dx.doi.org/10.1021/ic1024586 |Inorg. Chem. 2011, 50, 3501–3510

**Scheme 1. General Synthetic Route to the Polymeric Wires 1−3 with the Ligands Derived from Salicylic Acid Hydrazide and Aliphatic or Cycloaliphatic Ketones**

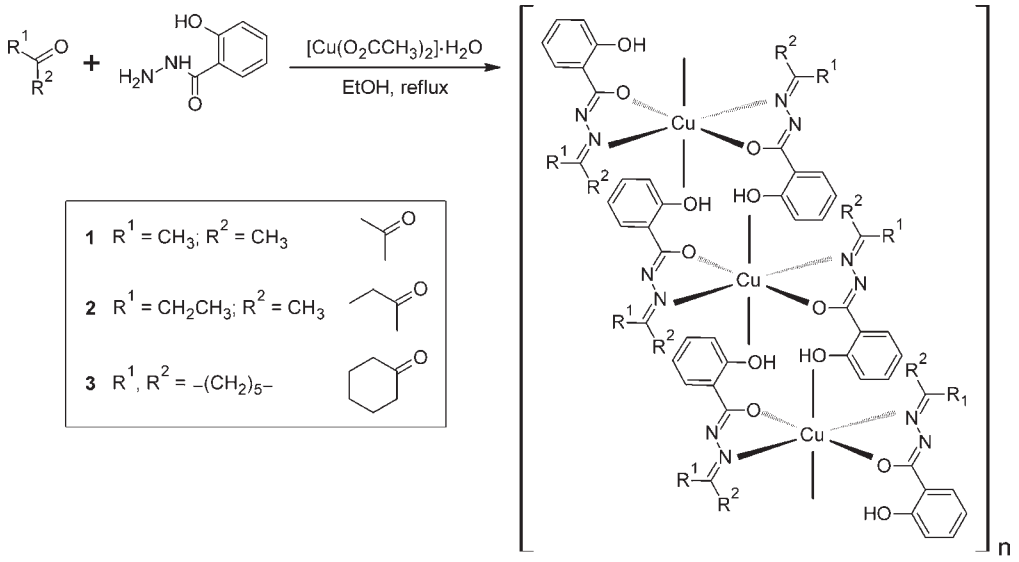


**Synthesis of $[Cu(\mu\text{-chesah})_2]_n \cdot nH_2O$ ($3 \cdot nH_2O$).** The synthetic procedure was analogous to that of **1**, except that cyclohexanone (210 $\mu$L, 2.00 mmol) was used instead of acetone. (Yield: 0.33 g; 62%) Anal. Calcd for $C_{26}H_{32}N_4O_5Cu$: C, 57.39; H, 5.93; N, 10.30. Found: C, 57.83; H, 5.54; N, 10.49%. IR (KBr, $cm^{-1}$): $\nu_{CN(imine)}$, 1594(vs), 1615(m); $\nu_{CO(enolate)}$, 1255(vs); $\nu_{CO(phenolic)}$, 1301(m). UV−vis (solid state) $\lambda$, nm: 600, 370(sh), 310, 270, 220. UV−vis [DMSO solution: $\lambda$, nm ($\varepsilon$, $dm^3\ mol^{-1}\ cm^{-1}$)]: 645 (100), 310 (2800).

**Synthesis of $[Cu(dbusah)_2] \cdot EtOH$ ($4 \cdot EtOH$).** The synthetic procedure was analogous to that of **1**, except that dibutylketone (345 $\mu$L, 2.00 mmol) was used instead of acetone. (Yield: 0.073 g; 11%) Anal. Calcd for $C_{34}H_{52}N_4O_5Cu$: C, 53.87; H, 4.97; N, 12.56. Found: C, 53.58; H, 4.94; N, 12.32%. IR (KBr, $cm^{-1}$): $\nu_{CN(imine)}$, 1601(vs); $\nu_{CO(enolate)}$, 1258(s); $\nu_{CO(phenolic)}$, 1307(s). UV−vis (solid state) ($\lambda$, nm): 550(broad), 370, 310, 260, 210. UV−vis [DMSO solution: $\lambda$, nm ($\varepsilon$, $dm^3\ mol^{-1}\ cm^{-1}$)]: 730 (63), 310 (20500). Greenish-gray crystals of **4** suitable for single-crystal XRD were obtained after recrystallization from MeCN.

## CRYSTALLOGRAPHIC DATA COLLECTION AND STRUCTURE REFINEMENT

The crystals of **1**, **2**, and **4** suitable for X-ray analysis were selected from the materials prepared as described in the Experimental Section. Intensity data for **1** and **2** were collected on an Oxford Diffraction SuperNova dual-source diffractometer with an Atlas electronic CCD area detector using Mova microfocus Mo K$\alpha$ radiation source ($\lambda$ = 0.71073 Å). Intensity data for **4** were collected on a Nonius Kappa CCD diffractometer, using graphite monochromated Mo K$\alpha$ radiation ($\lambda$ = 0.71073 Å). An Oxford Instruments Cryojet HT low-temperature device was used for cooling the crystal of **2** to 110 K. The crystal data, details of data collection and structure refinement parameters are summarized in Table 1. The positions of most atoms for all structures were determined by direct methods; other nonhydrogen atoms were located on difference Fourier maps. In complex **2**, methyl and ethyl groups were refined with fractional occupancy factors at two alternative positions. The displacement parameters of C15B indicated further disorder of ethyl group not resolved during refinement. Hydrogen H02 (**1** and **2**) and hydrogen H7 (**4**) were identified on difference Fourier maps and refined with geometrical restraints. All other hydrogen atoms bonded to carbons were included in the structure factor calculations at idealized positions.

The structures were solved using SIR92 and were refined using the SHELXL program.[15,16] Full crystallographic data may be obtained from the Cambridge Crystallographic Data Centre. The CCDC reference numbers are 818229 (**1**), 818230 (**2**), and 818231 (**4**).

## RESULTS AND DISCUSSION

**Synthetic Approach.** Our approach to synthesize salicyloyl hydrazone containing copper polymers utilizes a condensation reaction between a series of aliphatic/cycloaliphatic ketones (acetone, ethyl methyl ketone, cyclohexanone) and salicylic acid hydrazide. This reaction may be templated through the addition of copper(II) acetate to give $[Cu(\mu\text{-LL})_2]_n$ complexes **1**−**3**. It is likely that polymeric complexes with other metal centers may be synthesized using a similar strategy, which will be the subject of further studies. In this work, the appropriate precursors of Schiff bases were mixed in the equimolar amounts and subsequently reacted with copper(II) acetate in the molar ratio of 2:1 in refluxing EtOH. A general synthetic route to the polymeric copper wires **1**−**3** is presented in Scheme 1. It has been found that the use dibutyl ketone as a Schiff base component for the reaction with copper(II) acetate yields a monomeric $[Cu(LL)]_2$ complex **4**. Clearly, long alkyl chains here introduce a steric hindrance and prevent the polymerization of copper centers.

**Crystal Structures.** Compounds **1**−**3** possess six-coordinate copper centers that are doubly bridged by two salicyloyl hydrazone ligands in the $\mu_2-\eta^1,\eta^2$ coordination mode, whereas compound **4** contains four-coordinate central atoms each surrounded by two bidentate salicyloyl hydrazones, as confirmed by single-crystal X-ray structures of **1**, **2**, and **4**. The organic ligands in all compounds have undergone tautomerization and


dx.doi.org/10.1021/ic1024586 |*Inorg. Chem.* 2011, 50, 3501–3510

deprotonation in order to compensate the charge of the copper(II) centers on coordination. Thus, these Schiff bases are planar (except alkyl parts), because of the presence of conjugated double C═N bonds. The geometries at the metal centers are centrosymmetric for all compounds and the deprotonated Schiff base ligands are bound to the copper centers in the *trans*-N, O modes.

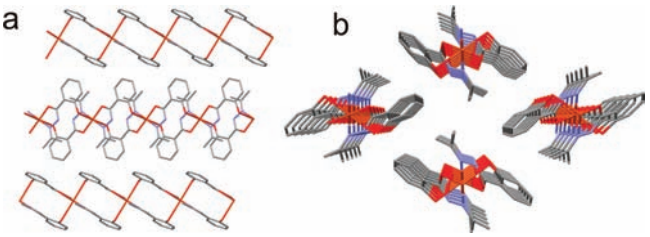


**Figure 1.** Single-crystal X-ray structure of $[Cu(\mu\text{-acesah})_2]_n$ (**1**), illustrating the packing pattern with a zigzag geometry of 1D nanowires, and viewed (a) perpendicular to a copper plane and (b) perspectively along the *a*-axis. Hydrogen atoms are omitted for clarity.

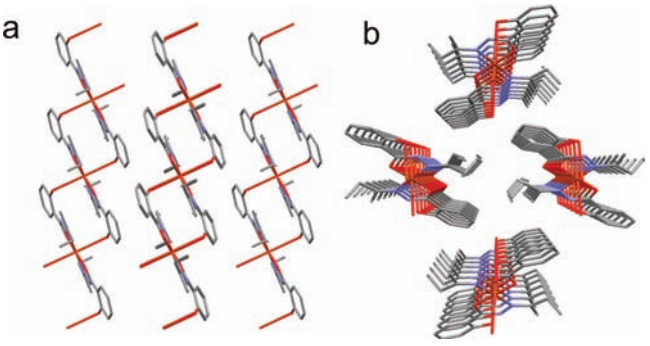


**Figure 2.** Single-crystal X-ray structure of $[Cu(\mu\text{-emsah})_2]_n$ (**2**), illustrating the packing pattern with a zigzag geometry of 1D nanowires, and viewed (a) along the *b*-axis and (b) perspectively along the *a*-axis. Hydrogen atoms are omitted for clarity.

Compounds **1** and **2** crystallize in monoclinic systems with space group of $P2_1/c$. Each unit cell contains $[Cu(\mu\text{-LL})_2]$ complexes, where LL are appropriate bridging $\mu_2-\eta^1,\eta^2$ salicyloyl hydrazone ligands: *N*-(propan-2-ylidene)-2-hydroxybenzenecarbohydrazonoate (acesah) and *N*-(butan-2-ylidene)-2-hydroxybenzenecarbohydrazonoate (emsah) for **1** and **2**, respectively. These Schiff base molecules link adjacent copper centers which leads to 1D metallopolymers. The packing patterns of both compounds in the solid state are illustrated in Figures 1 and 2. Each copper center is doubly bridged by the off-axis salicyloyl hydrazone linkers that exhibit a zigzag geometry. The polymeric chains, whose cross-sectional sizes are on the order of 1 nm, propagate along the [100] direction. These separate chains are related by a $2_1$ screw axis along the [010] direction. There are no cross-linking hydrogen bonds among chains, although there are such intrachain interactions between phenolic oxygen and salicyloyl hydrazone nitrogen atoms. The observed N10−O02 hydrogen bond distances are 2.577 Å (**1**) and 2.538 Å (**2**), respectively. The lack of interchain interactions results in fragility of these crystals; they are very brittle. It has been observed that exerting a relatively weak pressure on them leads to their destruction.

The structural motif of complex **1**, which resembles that of **2**, is depicted in Figure 3; selected bond distances and angles of **1** and **2** are listed in Table 2. Salicyloyl hydrazone ligands coordinate in a bidentate mode to the copper(II) to afford a Jahn−Teller distorted octahedral geometry. This distortion is related to the $d^9$ configuration of copper(II) centers. Equatorial positions are occupied by enolate oxygens and imine nitrogens of two bidentate salicyloyl deprotonated hydrazones, whereas the axial positions have phenolic oxygens that are substituents of aromatic rings of two other ligands bound to adjacent copper centers (see

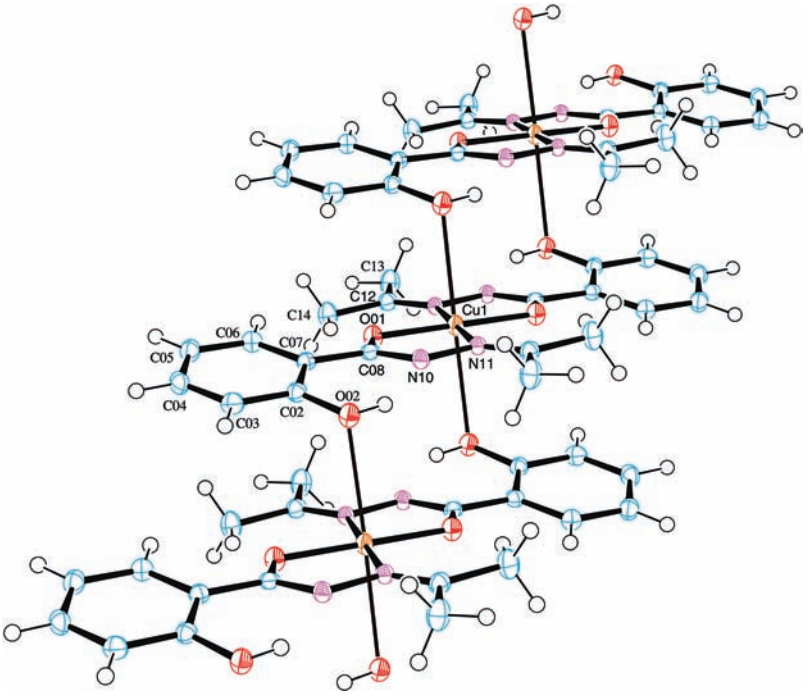


**Figure 3.** Single-crystal X-ray structure of $[Cu(\mu\text{-acesah})_2]_n$ (**1**) with the atom labeling scheme and 50% displacement ellipsoids.


dx.doi.org/10.1021/ic1024586 |*Inorg. Chem.* 2011, 50, 3501–3510

Scheme 1 and Figure 3). Planar Schiff bases occupying equatorial positions in complexes **1** and **2** form five-membered rings whose bite angles O01−Cu1−N11 [80.92° (**1**) and 81.33° (**2**)] are responsible for the deviation from ideal octahedral angles.

The observed Jahn−Teller distortions for both compounds are elongations along the axial axis (see Table 2). The comparison of bond distances between the two complexes shows the considerable difference in axial Cu1−O02 bonds. These are shorter (2.698 Å) for **1** than for **2** (2.789 Å), which may be due to the presence of a bulkier ethyl group in **2**. However, this longer distance observed for **2** does not translate to the intrachain Cu···Cu distances, which are even shorter for **2** (6.151 Å) than for **1** (6.220 Å). This can be explained by the considerable difference in bond angles between the complexes observed within their coordination polyhedra (see Table 2); the relevant O01−Cu1−O02 and O02−Cu1−N11 angles in complex **2** are smaller, by ∼3.8° and ∼1.6°, respectively. Except for the Cu1−O02 bonds, the rest of corresponding bond distances are the same or comparable in the two complexes. Both relatively long C08−O01 and short C08−N10 bond lengths in organic ligands demonstrate their enolate forms in both compounds (see Table 2).

**Table 2. Selected Bond Lengths and Angles for [Cu(*μ*-acesah)$_2$]$_n$ (1), [Cu(*μ*-emsah)$_2$]$_n$ (2), and [Cu(dbusah)$_2$] (4) (Estimated Standard Deviations Given in Parentheses)**

| | 1 | 2 | 4 |
|---|---|---|---|
| | | Bond Lengths (Å) | |
| Cu1−O01 | 1.909(1) | 1.903(2) | 1.891(2) |
| Cu1−O02 | 2.698(1) | 2.789(2) | |
| Cu1−N11 | 2.052(1) | 2.052(2) | 2.053(2) |
| C08−O01 | 1.285(2) | 1.283(3) | 1.286(3) |
| C08−N10 | 1.315(2) | 1.307(3) | 1.306(3) |
| N10−N11 | 1.407(2) | 1.406(3) | 1.404(3) |
| N11−C12 | 1.290(2) | 1.289(3) | 1.299(3) |
| O02−C02 | 1.362(2) | 1.356(4) | 1.344(4) |
| | | Bond Angles (deg) | |
| O01−Cu1−O02 | 87.38(5) | 83.57(7) | |
| O01−Cu1−O02′ | 92.62(5) | 96.43(7) | |
| O01−Cu1−N11 | 80.92(6) | 81.33(7) | 80.79(8) |
| O01−Cu1−N11′ | 99.08(5) | 98.67(7) | 99.21(8) |
| O02−Cu1−N11 | 88.41(5) | 86.88(7) | |
| O02−Cu1−N11′ | 91.59(5) | 93.12(7) | |
| O01−Cu1−O01′ | 180.00(5) | 180 | 180.000(1) |
| O02−Cu1−O02′ | 180 | 180 | |
| N11−Cu1−N11′ | 180.00(8) | 180.00(9) | 180.000(1) |

The structure of compound **4** is considerably different from those of **1** and **2**. It crystallizes in a triclinic system with a space group of $P\bar{1}$. Each unit cell contains a monomeric distorted square planar [Cu(LL)$_2$] complex where LL is a bidentate ligand, *N*-(nonan-5-ylidene)-2-hydroxybenzenecarbohydrazonoate (dbusah), bound to each central atom in the *trans*-N,O mode (see Figure 4). Similarly, as in the structures of **1** and **2**, bidentate Schiff bases in complex **4** form five-membered rings with bite angles of 80.79° and are responsible for the deviation from ideal square geometry. Unlike in complexes **1** and **2**, the long carbon chain of the butyl groups in complex **4** sterically hinders coordination of the copper(II) ions to the phenolic oxygen atoms of the ligands bound to adjacent copper centers. The packing pattern is presented in Figure 5, and the selected bond lengths and angles are listed in Table 2. Central copper atoms propagate along the [100] direction with intermetallic Cu···Cu distances of 8.122 Å, considerably longer than these in polymers **1** and **2** (see Figure 5). Alkyl chains of butyl groups separate these chains of discrete complexes with closest C···C distances of 4.122 Å. The rest of the corresponding bond distances in the structure of **4** are the same or comparable to those for complexes **1** and **2**. As in the structures of **1** and **2**, there are intramolecular hydrogen bonds between phenolic oxygen and salicyloyl hydrazone nitrogen atoms (2.575 Å), and both bidentate ligands are in

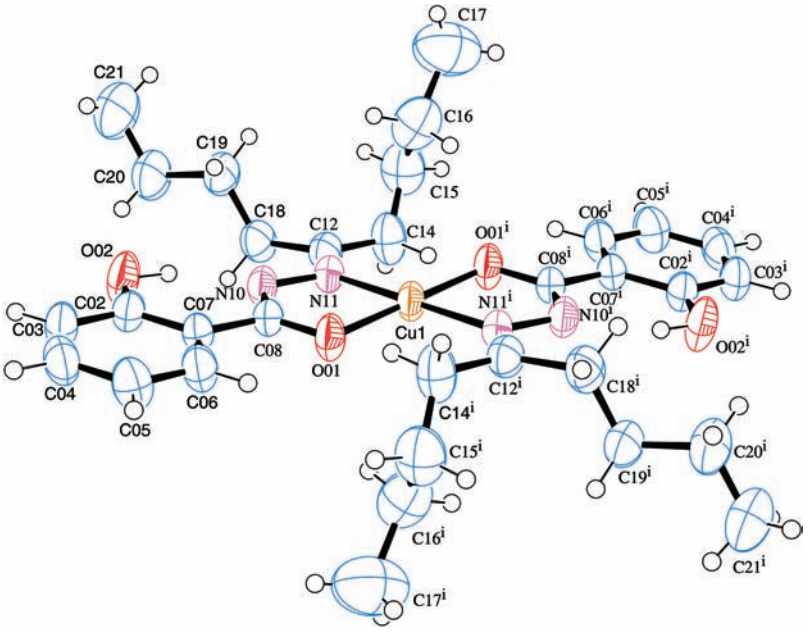


**Figure 4.** Single-crystal X-ray structure of [Cu(dbusah)$_2$] (**4**), showing the atom labeling scheme and 50% displacement ellipsoids.


dx.doi.org/10.1021/ic1024586 |*Inorg. Chem.* 2011, 50, 3501–3510

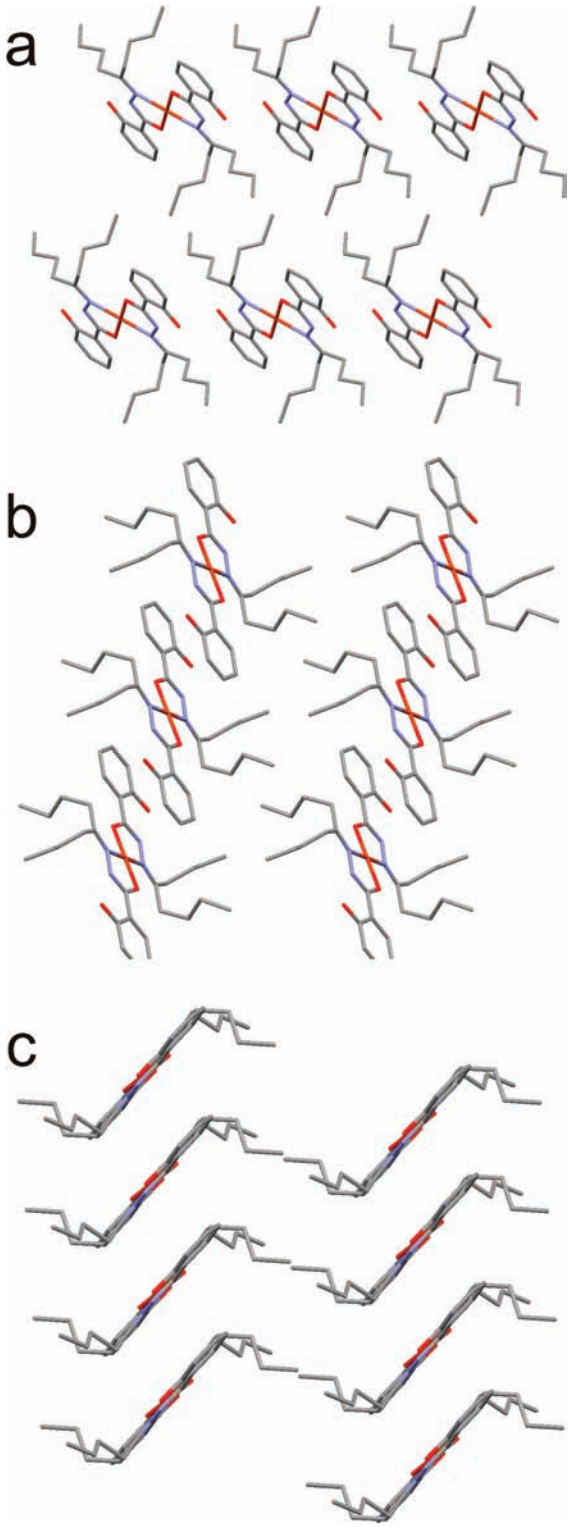


**Figure 5.** Single-crystal X-ray structure of $[Cu(dbusah)_2]$ (**4**), illustrating the packing pattern, and viewed (a) along the *a*-axis, (b) along the *b*-axis, and (c) along the $[\bar{1}\,1\,0]$ direction. Hydrogen atoms are omitted for clarity.

their enolate forms. Crystal structures of analogous mononuclear *trans*-$CuN_2O_2$ four-coordinate complexes with Schiff bases derived from salicyl- or hydroxynaphthalenecarbox-aldehydes and bulky amines (1-ethylpropylamine, 1-naphthylethylamine,

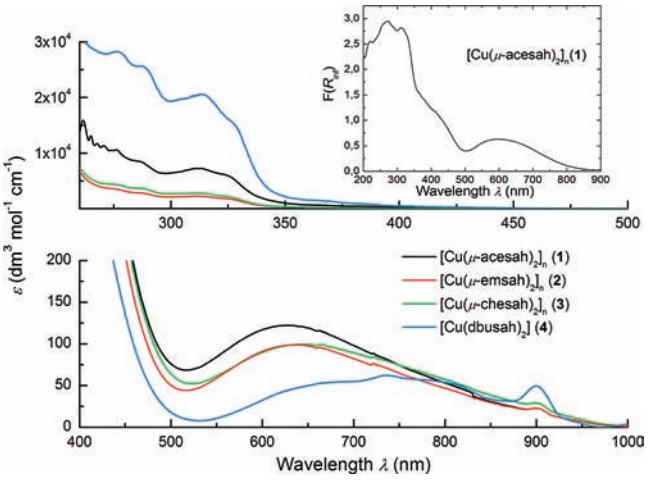


**Figure 6.** UV−visible absorption spectra of **1**−**4** in DMSO. The diffuse reflectance spectrum of **1** is given for comparison.

1-phenylethylamine, or cycloamines) exhibited mostly geometries that are intermediate between square planar and tetrahedral.[17] Generally, these configurations are dependent on the substituents at the nitrogen atom exhibiting different steric effects.[18]

**Spectroscopic and Magnetic Properties.** The infrared spectroscopic data of the Cu(II) complexes exhibit several characteristic absorptions for organic ligands.[19] The presence of the azomethine group in all complexes is conspicuous by the $\nu$(C═N) absorptions that appear as strong bands at ca. 1600 $cm^{-1}$. Ring-breathing vibrations of the aromatic rings of the appropriate ligands range from 1420 $cm^{-1}$ to 1560 $cm^{-1}$. The infrared spectra of **1**−**4** also exhibit absorption bands characteristic for C−O groups, as well as those assignable to both aliphatic and aromatic C−H vibrations. Strong signals at ∼1260 $cm^{-1}$ indicate the presence of enolate C−O groups, whereas the absorptions at ∼1300 $cm^{-1}$ are typical for phenolic C−O moieties. The position of the latter is similar for all complexes but one. This clearly distinguishable signal, observed relatively high at 1329 $cm^{-1}$ for compound **2**, indicates a stronger phenolic C−O bond in comparison with the other complexes and is in agreement with the structural data for **1** and **2**. The C−H bonds of the alkyl groups of **1**−**4** are readily identifiable by their absorptions in the 2840−2960 $cm^{-1}$ region, whereas the aromatic C−H vibrations of organic ligands occur at ∼3030−3060 $cm^{-1}$. The lack of characteristic N−H (ca. 3300 $cm^{-1}$) stretching vibrations as well as those of secondary amides at ∼1650 $cm^{-1}$ (C═O) additionally confirms the enolizations of salicyloyl hydrazone ligands. Wide absorptions at ∼3400 $cm^{-1}$ observed for all complexes are attributable to O−H stretching vibrations.

The magnetic susceptibility measurements were performed for all compounds at room temperature. The observed effective magnetic moments: 1.9 $\mu_B$ (**1**), 1.7 $\mu_B$ (**2**), 1.5 $\mu_B$ (**3**), and 1.8 $\mu_B$ (**4**) (without the corrections for diamagnetism) are comparable to the expected spin-only value (1.73 $\mu_B$) for one unpaired electron and confirm the formal +2 oxidation state of the copper centers.

The reflectance UV−vis spectra of **1**−**4** contain bands in the 200−400 nm region that are attributable to intraligand CT transitions, as well as broad bands of the lowest energies at ∼550−600 nm assignable to *d*−*d* transitions. The electronic absorption spectra of these compounds dissolved in DMSO are presented in Figure 6, together with the representative diffuse


dx.doi.org/10.1021/ic1024586 |*Inorg. Chem.* 2011, 50, 3501–3510

**Table 3. Selected Electrode Potentials ($E$) and Peak-to-Peak Separations ($\Delta E$) for the Anodic and Cathodic Processes Exhibited by Complexes 1−4 in DMSO Solutions**

| complex[a] | $^1E_{pc}$ (V vs SHE) | $^1E_{pa}$ (V vs SHE) | $^1E_{1/2}$ (V vs SHE) | $^1\Delta E$ (V) | $^2E_{pc}$ (V vs SHE) | $^2E_{pa}$ (V vs SHE) | $^2E_{1/2}$ (V vs SHE) | $^2\Delta E$ (V) | $^3E_{pc}$ (V vs SHE) |
|---|---|---|---|---|---|---|---|---|---|
| **1** | 0.075 | 0.27(sh) | 0.17 | 0.19 | −0.085 | 0.36 | 0.14 | 0.45 | −0.90[b] |
| **2** | 0.11 | 0.27[c] | 0.19 | 0.16 | −0.10 | 0.27[c] | | | −0.82[b] |
| **3** | 0.15 | 0.38[c] | | | −0.10 | 0.38[c] | 0.14 | 0.48 | −0.68[b] |
| **4** | 0.20[b] | 0.37[b] | 0.28[b] | 0.17[b] | −0.11[b] | | | | −0.82[b] |

[a] Measurements for **1**−**3** are carried out at as multicycles at 50 mV $s^{-1}$, and the data correspond to their voltammograms in Figure 7. [b] Data obtained from single measurement at 200 mV $s^{-1}$. [c] Broad unresolved signal.

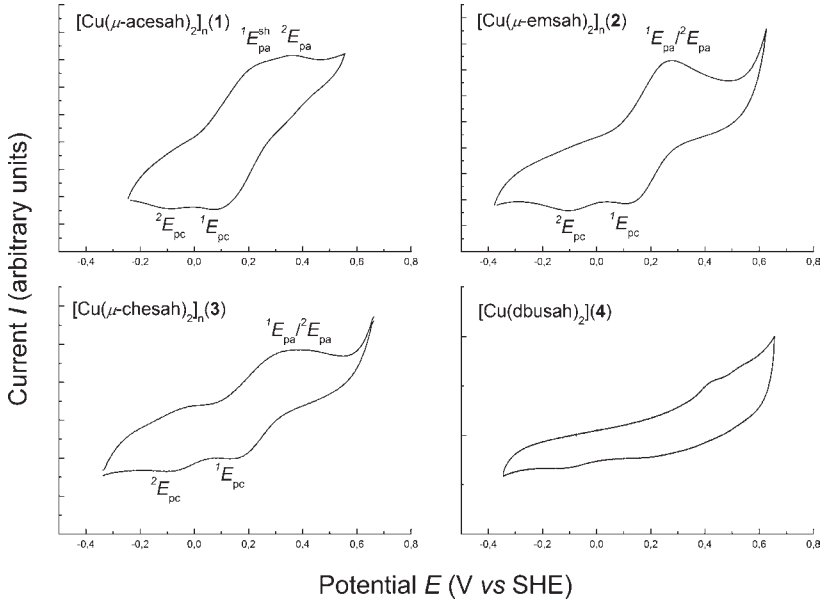


**Figure 7.** Cyclic voltammograms measured in DMSO solutions for (top left) **1** after 9 cycles at a can speed of 50 mV $s^{-1}$, (top right) **2** after 4 cycles at a can speed of 50 mV $s^{-1}$, (bottom left) **3** after 4 cycles at a can speed of 50 mV $s^{-1}$, and (bottom right) **4** after 9 cycles at a can speed of 200 mV $s^{-1}$.

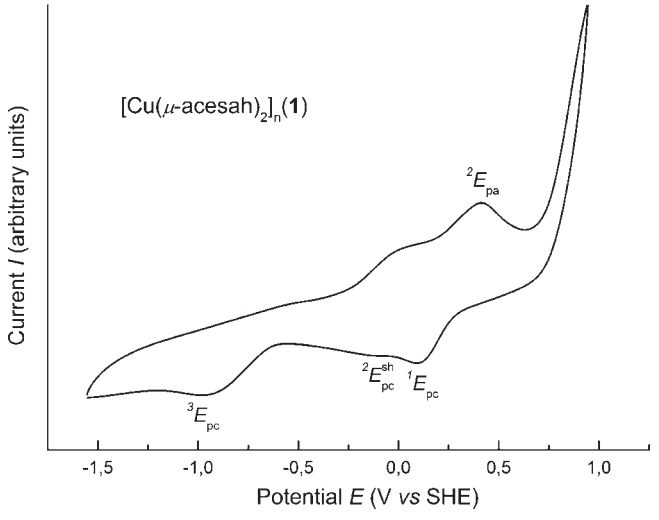


**Figure 8.** Cyclic voltammogram measured in DMSO solution for **1** at 200 mV $s^{-1}$ within a potential range from −1.55 V to 0.95 V.

reflectance spectrum of **1**. Similarly, as in the solid state, the UV region of each spectrum is dominated by absorption bands in the ranges of 250−420 nm, which are attributable to ligand-to-metal

**Scheme 2. Electrochemical and Chemical Processes in DMSO Solutions of Complexes 1−3**

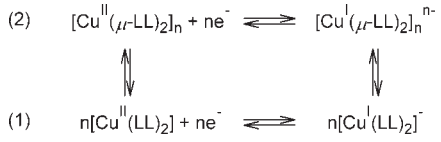


CT transition and the electronic transitions of the organic ligands.[11a] The visible region for complexes **1**−**3** exhibits weak absorptions in the range of 628−645 nm associated with $d-d$ transitions, which is consistent with related complexes.[5,6] On the other hand, the $d-d$ transitions of the complex **4** are represented by the broad absorption band at ∼730 nm with several weakly pronounced shoulders, some of them being instrument artifacts. Nevertheless, the visible spectra of the six-coordinate complexes (**1**−**3**) are significantly different from that of the square planar complex **4**, which indicates structural differences at the metal center and confirms the findings of X-ray crystallography. The unresolved broad absorption observed for complex **4** contains at least two overlapping bands corresponding to the $^2B_{1g} \rightarrow {}^2B_{2g}$ and $^2B_{1g} \rightarrow {}^2E_g$ transitions. The same transitions should be observed for **1**−**3**, since all complexes **1**−**4** possess the same $D_{4h}$


dx.doi.org/10.1021/ic1024586 |Inorg. Chem. 2011, 50, 3501–3510

symmetry. However, the separation of excited states $^2B_{2g}$ and $^2E_g$ is much smaller in the case of a tetragonally elongated octahedral geometry than in the case of a square planar geometry; therefore, the visible spectra of complexes **1**−**3** exhibit narrower, unsymmetrical bands that correspond to the two transitions.

**Cyclic voltammetry.** The cyclic voltammograms for all copper(II) complexes **1**−**4** were recorded at various scan speeds (50−1000 mV $s^{-1}$) over the range from −1500 mV to 1000 mV (versus Ag/AgCl) in DMSO, and the electrochemical data are summarized in Table 3. The representative voltammograms for all complexes are presented in Figures 7 and 8.

All of the complexes except **4** show similar electrochemical behaviors. Their voltammograms display, within scan speeds of 50−200 mV $s^{-1}$, two reduction waves ($^1E_{pc}$ and $^2E_{pc}$), which occur in the potential ranges from 75 mV to 150 mV and from −175 mV to −85 mV, respectively (see Figure 7). The first quasi-reversible reduction wave corresponds to the $[Cu^{II}(LL)_2]/[Cu^{I}(LL)_2]^-$ process (1), with a directly associated reoxidation peak ($^1E_{pa}$) in the reverse scan, whose potential values are in the range of 270−380 mV (see Table 3). The second quasi-reversible reduction wave ($^2E_{pc}$), with its back wave ($^2E_{pa}$) in the reverse scan, is interpreted as the $[Cu^{II}(\mu\text{-LL})_2]_n/[Cu^{I}(\mu\text{-LL})_2]_n^{n-}$ process (2) with relatively high peak separations, which is typical when CT involves polymeric species. This back signal is observed either as a broad unresolved anodic wave (for complexes **2** and **3**) or as a wave with a shoulder (complex **1**). The presence of two reduction waves with related two oxidation signals in the relatively narrow range of potentials (within a range from −0.2 V to 0.6 V) in DMSO solutions of polymeric complexes **1**−**3** can be explained by the presence of another copper(II) species, most probably monomeric complexes (see Scheme 2). In addition, the variations of scan speeds in multicyclic measurements over this narrow range of potentials allows one to observe different changes in diffusion currents that accompany processes (1) and (2) (see Figure 9), thus supporting their interpretation and labeling. The dependence of $^1I$ and $^2I$ current values on scan speed (see Figure 9) indicates the possible interconversions between polymeric and monomeric species in solution (see Scheme 2). Thus, processes (1) and (2) are associated with monomers and polymers, respectively. Polymeric forms of complexes seem to undergo relatively slow depolymerization process upon reduction. Thus, at low scan speeds, signals related to monomeric oxidation/reduction are more distinct; at higher scan speeds, these waves are less pronounced, because smaller amounts of monomeric forms are generated near the electrode surface (see Figure 9).

The reduction potentials $^1E_{pc}$ (for monomers) become considerably more positive as the ketone alkyl substituents become bulkier in the following order: acetone < ethylmethyl ketone < cyclohexanone < dibutyl ketone. These results are in agreement with those presented by Patterson and Holm,[20] who studied copper(II) chelates with alkyl substituents but remain in contrast with those presented by Fernandez et al. for the series of $CuN_2O_2$ chelates with cycloalkyl substituents.[17e] The first authors explained the effect as the result of complex geometry changes going from square planar ones with less bulky substituents to tetrahedrally distorted ones as the bulkiness of substituents increases. However, this explanation cannot account for our findings for the series of complexes **1**−**4**, because all of their bischelate geometries around metal centers are approximately planar. Most probably, the observed trend is associated with increasing electro-donating character of alkyl groups with their bulkiness, which makes their copper(II) complexes easier to reduce. On the other hand, the explanation of the reverse trend by Fernandez et al., who associated the bulkiness of substituents with the difficulty involved in approaching the electrode, is consistent with the values of $^2E_{pc}$ reduction potentials (see Table 3), relative to polymeric forms; however, this trend is not so distinct.

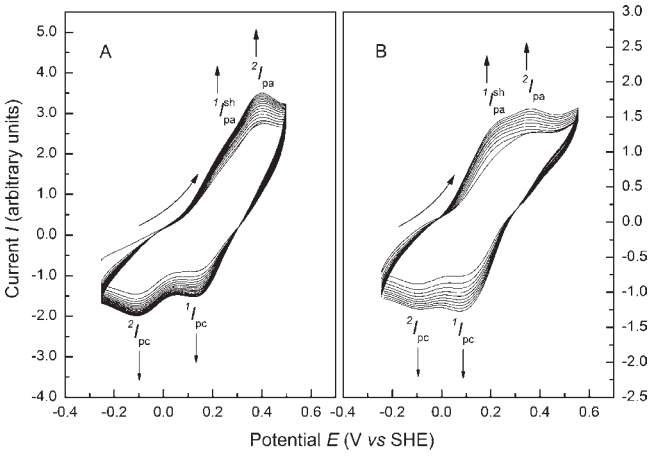


**Figure 9.** Formation of the polymeric film of the complex $[Cu(\mu\text{-acesah})_2]_n$ (**1**). Multiscan cycles recorded within −0.25 V to 0.50 V: (A) 15 cycles at 200 mV $s^{-1}$ and (B) 10 cycles at 50 mV $s^{-1}$.

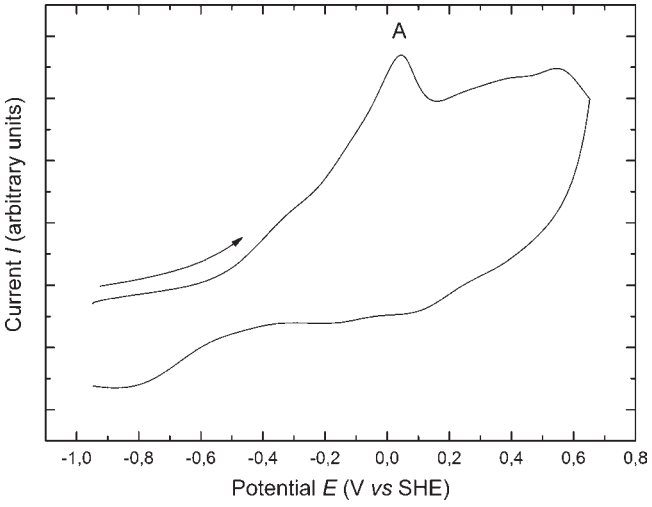


**Figure 10.** Current response as a function of applied potential at 200 mV $s^{-1}$ for a Pt electrode in contact with DMSO solution of complex $[Cu(\mu\text{-emsah})_2]_n$ (**2**) measured after 60 s of microelectrolysis at −0.95 V.

It is also noteworthy that, for polymeric complexes **1**−**3**, multiscan potential sweeps within the range of reduction $^1E_{pc}$, $^2E_{pc}$ and oxidation $^1E_{pa}$, $^2E_{pa}$ processes result in the steady increase in the currents of the anodic and cathodic peaks (see Figure 9). It indicates that conducting films of polymeric copper complexes are formed on the working electrode surface.[21] No such behavior is observed for the monomeric complex $[Cu(dbusah)_2]$ (**4**), where multiscan sweeps make all signals become smaller with each cycle until no distinct signals are finally observed. The formation of a conducting film on a Pt electrode was recently reported for monomeric Cu(II) complex with a tetradentate Schiff base derived from 1,3-propylenediamine and 3-methoxysalicylaldehyde, where


dx.doi.org/10.1021/ic1024586 |*Inorg. Chem.* 2011, 50, 3501–3510

two models of electropolymerization were proposed.[22] In contrast to that report, here, we were unable to deposit such a conducting film starting from a monomeric complex **4**.

All complexes exhibit a broad reduction wave $^3E_{pc}$ in the range from −680 mV to −900 mV (at a scan speed of 100 mV $s^{-1}$), attributable to the $[Cu^I(LL)_2]/[Cu^0(LL)_2]^-$ or $[Cu^I(\mu\text{-}LL)_2]_n/n[Cu^0(\mu\text{-}LL)_2]^-$ processes lacking a directly associated response in the reverse scan, because of the rapid decomposition of $Cu^0$ complexes to metallic copper with the ligand release. This was confirmed when the microelectrolyses for 60 s at a low potential, close to the observed reduction waves ($^3E_{pc}$), were carried out, and, in the reverse scan, the "stripping-like" anodic peak A appeared to be associated with the reoxidation of electrodeposited copper to free $Cu^+$ ion. The representative voltammogramm is presented in Figure 10.

## CONCLUDING REMARKS

It has been shown, in this work, that the complexation of copper(II) with a series of derivatives of salicylic acid hydrazide and aliphatic or cycloaliphatic ketones leads either to one-dimensional (1D) metallopolymers containing Schiff bases (LL) as bridging $\mu_2-\eta^1,\eta^2$ ligands or four-coordinate $[Cu(LL)_2]$ monomers, depending on the ketone used. Single-crystal X-ray diffraction (XRD) results have revealed nanometer-sized polymeric copper chains $[Cu(\mu\text{-}LL)_2]_n$ with off-axis linkers and a zigzag geometry, as well as square planar geometry of the monomers.

This report on a bottom-up formation of soluble single-chain copper-organic backbones based on salicyloyl hydrazones may serve as a basis for future investigations of coordination polymers with such ligands. In particular, it opens new attractive routes for the creation of novel supramolecular structures with desirable properties such as pore shape, size, composition, and function.

## ASSOCIATED CONTENT

**Supporting Information.** CIF files for **1**, **2**, and **4**. This material is available free of charge via the Internet at http://pubs.acs.org.

## AUTHOR INFORMATION

**Corresponding Author**

*Tel.: +4812-6632223. Fax: +4812-6340515. E-mail: matoga@chemia.uj.edu.pl.

## ACKNOWLEDGMENT

The research was carried out with the equipment purchased thanks to the financial support of the European Regional Development Fund in the framework of the Polish Innovation Economy Operational Program (Contract No. POIG.02.01.00-12-023/08).

## REFERENCES

(1) See for example:(a) *Crystal Design: Structure and Function*. Vol. 7; Desiraju, G. R., Ed.; John Wiley & Sons, Ltd.: Chichester, U.K., 2003. (b) Gasnier, A.; Barbe, J.-M.; Bucher, C.; Duboc, C.; Moutet, J.-C.; Saint-Aman, E.; Terech, P.; Royal, G. *Inorg. Chem.* **2010**, *49*, 2592–2599. (c) Friese, V. A.; Kurth, D. G. *Coord. Chem. Rev.* **2008**, *252*, 199–211. (d) Kurth, D. G.; Higuchi, M. *Soft Matter* **2006**, *2*, 915–927. (e) Lin, X.; Jia, J.; Zhao, X.; Thomas, K. M.; Blake, A. J.; Walker, G. S.; Champness, N. R.; Hubberstey, P.; Schroder, M. *Angew. Chem., Int. Ed.* **2006**, *45*, 7358–7364. (f) Hoogenboom, R.; Schubert, U. S. *Chem. Soc. Rev.* **2006**, *35*, 622–629. (g) Hofmeier, H.; Schubert, U. S. *Chem. Commun.* **2005**, 2423–2432. (h) Oh, M.; Mirkin, C. A. *Nature* **2005**, *438*, 651–654. (i) Vermonden, T.; Van Der Gucht, J.; De Waard, P.; Marcelis, A. T. M.; Besseling, N. A. M.; Sudholter, E. J. R.; Fleer, G. J.; Stuart, M. A. C. *Macromolecules* **2003**, *36*, 7035–7044. (j) Janiak, C. *Dalton Trans.* **2003**, 2781–2804. (k) Brunsveld, L.; Folmer, B. J. B.; Meijer, E. W.; Sijbesma, R. P. *Chem. Rev.* **2001**, *101*, 4071–4097. (i) Moulton, B.; Zaworotko, M. J. *Chem. Rev.* **2001**, *101*, 1629–1658.

(2) (a) Holliday, B. J.; Swager, T. M. *Chem. Commun.* **2005**, 23–36. (b) Whittel, G. R.; Manners, I. *Adv. Mater.* **2007**, *19*, 3439–3468. (c) Eloi, J.-C.; Chabanne, L.; Whittel, G. R.; Manners, I. *Mater. Today* **2008**, *11*, 28–36. (d) Mortimer, R. J.; Dyer, A. L.; Reynolds, J. R. *Displays* **2006**, *27*, 2–18. (e) Wolf, M. O. *Adv. Mater.* **2001**, *13*, 545–553.

(3) (a) Leung, A. C. W.; Hui, J. K.-H.; Chong, J. H.; MacLachlan, M. J. *Dalton Trans.* **2009**, 5199–5210. (b) Leung, A. C. W.; MacLachlan, M. J. *J. Inorg. Organomet. Polym. Mater.* **2007**, *17*, 57–89.

(4) Buvailo, A. I.; Gumienna-Kontecka, E.; Pavlova, S. V.; Fritsky, I. O.; Haukka, M. *Dalton Trans.* **2010**, *39*, 6266–6275.

(5) Ranford, J. D.; Vittal, J. J.; Wang, Y. M. *Inorg. Chem.* **1998**, *37*, 1226–1231.

(6) Sangeetha, N. R.; Pal, S. *Polyhedron* **2000**, *19*, 1593–1600.

(7) Li, R.; Moubaraki, B.; Murray, K. S.; Brooker, S. *Dalton Trans.* **2008**, 6014–6022.

(8) (a) Naiya, S.; Biswas, C.; Drew, M. G. B.; Gomez-Garcia, C. J.; Clemente-Juan, J. M.; Ghosh, A. *Inorg. Chem.* **2010**, *49*, 6616–6627. (b) Tandon, S. S.; Bunge, S. D.; Motry, D.; Costa, J. S.; Aromi, G.; Reedijk, J.; Thompson, L. K. *Inorg. Chem.* **2009**, *48*, 4873–4861.

(9) (a) Jia, L.; Jiang, P.; Xu, J.; Hao, Z.; Xu, X.; Chen, L.; Wu, J.; Tang, N.; Wang, Q.; Vittal, J. J. *Inorg. Chim. Acta* **2010**, *363*, 855–865. (b) Jia, L.; Tang, N.; Vittal, J. J. *Inorg. Chim. Acta* **2009**, *362*, 2525–2528. (c) Wang, X.; Ranford, J. D.; Vittal, J. J. *J. Mol. Struct.* **2006**, *796*, 28–35. (d) Yang, C. T.; Moubaraki, B.; Murray, K. S.; Ranford, J. D.; Vittal, J. J. *Inorg. Chem.* **2001**, *40*, 5934–5941.

(10) (a) Nagarathinam, M.; Saravanan, K.; Leong, W. L.; Balaya, P.; Vittal, J. J. *Cryst. Growth Des.* **2009**, *9*, 4461–4470. (b) Nagarathinam, M.; Chen, J.; Vittal, J. J. *Cryst. Growth Des.* **2009**, *9*, 2457–2463.

(11) (a) Ainscough, E. W.; Brodie, A. M.; Dobbs, A. J.; Ranford, J. D.; Waters, J. M. *Inorg. Chim. Acta* **1998**, *267*, 27–38. (b) Ainscough, E. W.; Brodie, A. M.; Denny, W. A.; Finlay, G. J.; Gothe, S. A.; Ranford, J. D. *J. Inorg. Biochem.* **1999**, *77*, 125–133. (c) Chan, S. C.; Koh, L. L.; Leung, P. H.; Ranford, J. D.; Sim, K. Y. *Inorg. Chim. Acta* **1995**, *236*, 101–108.

(12) (a) Johnson, D. K.; Murphy, T. B.; Rose, N. J.; Goodwin, W. H.; Pickart, L. *Inorg. Chim. Acta* **1982**, *67*, 159–165. (b) Pickart, L.; Goodwin, W. H.; Burgua, W.; Murphy, T. B.; Johnson, D. K. *Biochem. Pharmacol.* **1983**, *32*, 3868–3871. (c) Aruffo, A. A.; Murphy, T. B.; Johnson, D. K.; Rose, N. J.; Schomaker, V. *Inorg. Chim. Acta* **1982**, *67*, L25–L27.

(13) Smith, P. A. S. *Org. Synth.* **1956**, *36*, 69.

(14) Supniewski, J. *Preparatyka nieorganiczna*; PWN: Warszawa, Poland, 1985; p 693.

(15) Altomare, A.; Cascarano, G.; Giacovazzo, G.; Guagliardi, A.; Burla, M. C.; Polidori, G.; Camalli, M. *J. Appl. Crystallogr.* **1994**, *27*, 435.

(16) Sheldrick, G. M. *Acta Crystallogr., Sect. A: Found. Crystallogr.* **2008**, *A64*, 112.

(17) (a) Fernandez-G., J. M.; Ausbun-Valdes, C.; Gonzalez-Guerrero, E. E.; Toscano, R. A. *Z. Anorg. Allg. Chem.* **2007**, *633*, 1251–1256. (b) Iglesias, A. L.; Aguirre, G.; Somanathan, R.; Parra-Hake, M. *Acta Crystallogr., Sect. E: Struct. Rep. Online* **2006**, *62*, o390–o392. (c) Iglesias, A. L.; Aguirre, G.; Somanathan, R.; Parra-Hake, M. *Polyhedron* **2004**, *23*, 3051–3062. (d) Fernandez-G., J. M.; Lopez-Duran, F. A.; Hernandez-Ortega, S.; Gomez-Vidales, V.; Macias-Ruvalcaba, N.; Aguilar-Martinez, M. *J. Mol. Struct.* **2002**, *612*, 69–79. (e) Aguilar-Martinez, M.; Saloma-Aguilar, R.; Macias-Ruvalcaba, N.; Cetina-Rosado, R.; Navarette-Vazquez, A.; Gomez-Vidales, V.; Zentella-Dehesa, A.;

Toscano, R. A.; Hernandez-Ortega, S.; Fernandez-G., J. M. *Dalton Trans.* **2001**, 2346–2352.
(18) Garnovskii, A. D.; Vasil'chenko, I. S. *Russ. Chem. Rev.* **2002**, *71*, 943–968.
(19) Bellamy, R. L. *The Infra-red Spectra of Complex Molecules*, Vol. 1; Chapman and Hall: London, 1975.
(20) Patterson, G. S.; Holm, R. H. *Bioinorg. Chem.* **1975**, *4*, 257–275.
(21) Heinze, J.; Frontana-Uribe, B. A.; Ludwigs, S. *Chem. Rev.* **2010**, *110*, 4724–4771.
(22) Borisov, A. N.; Shchukarev, A. V.; Shagisultanova, G. A. *Russ. J. Appl. Chem.* **2009**, *82*, 1242–1250.